Managing radiation degradation of CCDs on the Chandra X-ray Observatory

Stephen L. O'Dell[a], William C. Blackwell[b], Robert A. Cameron[c], Joseph I. Minow[b], David C. Morris[c,d], Bradley J. Spitzbart[c], Douglas A. Swartz[e], Shanil N. Virani[c], and Scott J. Wolk[c]

[a] NASA Marshall Space Flight Center, MSFC/SD50
Huntsville, AL 35812 USA
[b] Jacobs Sverdrup, MSFC/ED44
Huntsville, AL 35812 USA
[c] Harvard–Smithsonian Center for Astrophysics, 60 Garden Street
Cambridge, MA 02138 USA
[d] Penn State, Department of Astronomy & Astrophysics, 525 Davey Lab.
University Park, PA 16802 USA
[e] Universities Space Research Association, MSFC/SD50
Huntsville, AL 35812 USA

ABSTRACT

The CCDs on the *Chandra X-ray Observatory* are sensitive to radiation damage, particularly from low-energy protons scattering off the telescope's mirrors onto the focal plane. In its highly elliptical orbit, *Chandra* passes through a spatially and temporally varying radiation environment, ranging from the radiation belts to the solar wind. Translating the Advanced CCD Imaging Spectrometer (ACIS) out of the focal position during radiation-belt passages has prevented loss of scientific utility. However, carefully managing the radiation damage during the remainder of the orbit, without unnecessarily sacrificing observing time, is essential to optimizing the scientific value of this exceptional observatory throughout its planned 10-year mission. In working toward this optimization, the *Chandra* team developed and applied a radiation-management strategy. This strategy includes autonomous instrument safing triggered by the on-board radiation monitor, as well as monitoring, alerts, and intervention based upon real-time space-environment data from NOAA and NASA spacecraft. Furthermore, because *Chandra* often spends much of its orbit out of the solar wind (in the Earth's outer magnetosphere and magnetosheath), the team developed the *Chandra* Radiation Model to describe the complete low-energy-proton environment. Management of the radiation damage has thus far succeeded in limiting degradation of the charge-transfer inefficiency (CTI) to less than 3.5×10^{-6} and 1.3×10^{-6} per year for the front-illuminated and back-illuminated CCDs, respectively. This rate of degradation is acceptable for maintaining the scientific viability of all ACIS CCDs for more than ten years.

1. INTRODUCTION

The *Chandra X-ray Observatory*[1,2] — nee the Advanced X-ray Astrophysics Facility (AXAF) — provides unprecedented high-resolution imaging and spectroscopy of celestial x-ray sources. Principal observatory components are its subarcsecond-resolution x-ray optics, two interchangeable objective transmissions gratings (OTGs), and two interchangeable focal-plane imaging instruments. Each focal-plane instrument comprises two sets of detectors — one optimized for direct imaging, the other for read-out of the OTG-dispersed spectra. The High-Resolution Camera[3,4] — HRC, developed by the Smithsonian Astrophysical Observatory (SAO) — uses microchannel plates (MCPs); the Advanced CCD Imaging Spectrometer[5,6] — ACIS (Figure 1), developed by Pennsylvania State University (PSU) and the Massachusetts Institute of Technology (MIT) — uses charge-coupled devices (CCDs).

Contact information:
S.L.O.: E-mail = Steve.O'Dell@msfc.nasa.gov; Phone = +1(256)961-7776.

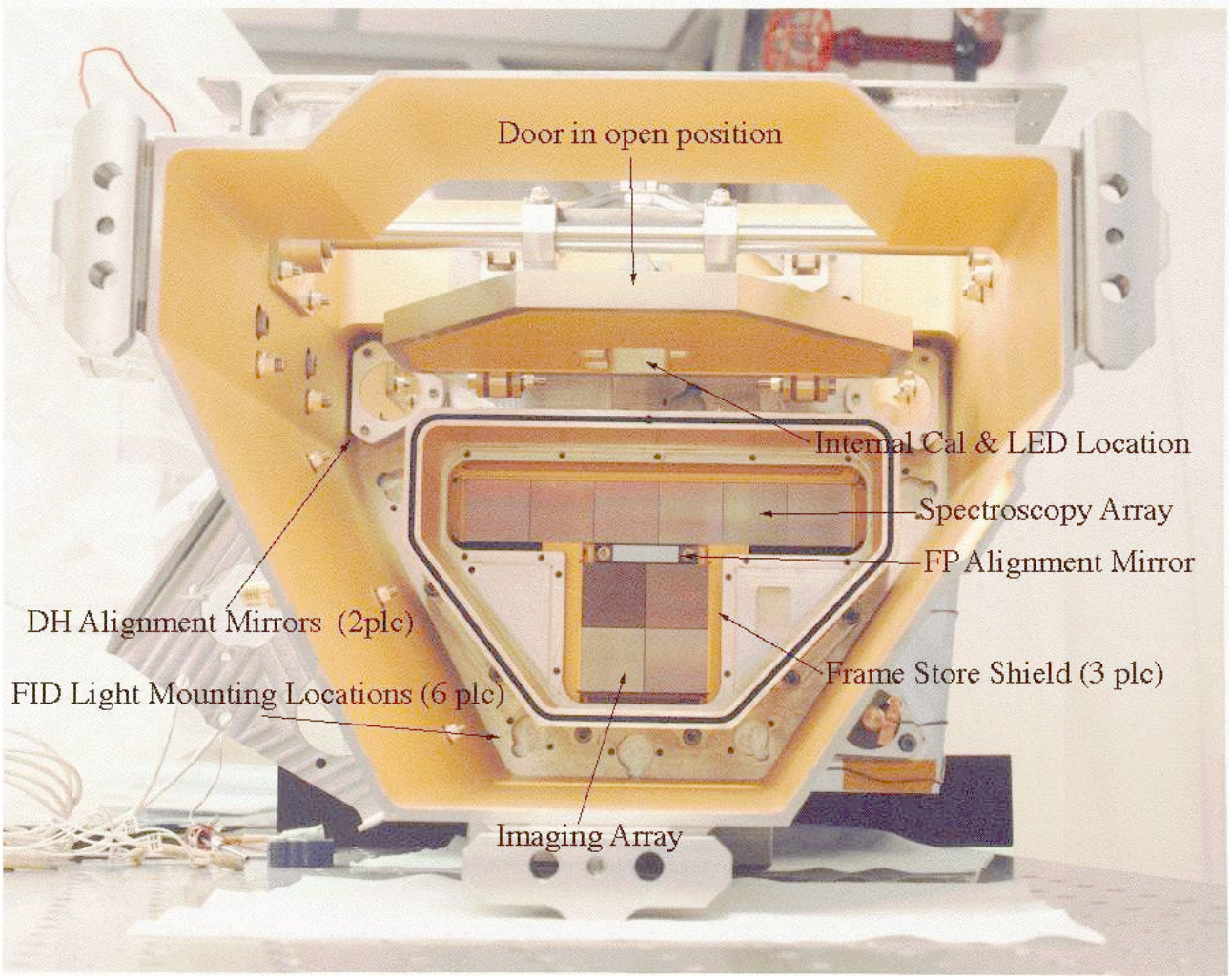

Figure 1. Photograph of ACIS, showing CCDs without optical blocking filter. The 2×2-CCD I-array serves as a wide-field spectrometric imager; the 1×7-CCD S-array, as a grating-spectroscopy read-out. Two of the S-array CCDs — S1 and S3 (second and fourth from right in this picture) — are back-illuminated; all other CCDs are front-illuminated. Owing to its superior low-energy response, S3 also serves as a narrow-field spectrometric imager. [PSU&MIT/ACIS]

On 1999 August 12, about 3 weeks after its launch on July 23 into a high elliptical orbit (140-Mm apogee, 10-Mm perigee altitude), the observatory's forward cover opened, exposing the *Chandra* focal plane to cosmic x rays and to the space environment. About a month after door opening, analysis of ACIS data discerned a marked increase in the charge-transfer inefficiency (CTI) of the front-illuminated CCDs. Fortunately, the *Chandra* team soon determined the cause of this CTI anomaly — radiation damage by low-energy protons, occurring predominantly in the Earth's outer proton radiation belt. The *Chandra* team immediately revised operating procedures to ensure that ACIS is always stowed in the next-in-line (NIL) position during passage through the inner magnetosphere, thus halting the rapid degradation of the CTI of the CCDs. We then developed a mitigation strategy to manage the residual radiation degradation throughout the life of the mission.

Here, we review the CTI anomaly (§2) and the radiation-management strategy (§3) that has successfully reduced the rate of CTI increase. Next, we describe the *Chandra* Radiation Model (CRM, §4), developed for planning and for real-time estimation of the low-energy-proton environment in *Chandra*'s orbit. We then present a case study of a recent proton event (§5), illustrating some real-time tools used in radiation protection. Finally, we report the current status of CTI and compare it to the CRM-estimated proton fluence (§6).

2. CTI ANOMALY AND RESOLUTION

We briefly summarize our previous report[7] on the ACIS CTI anomaly, its cause, and its resolution. During the first 8 unprotected radiation-belt passes, the (parallel-transfer) CTI of ACIS's 8 front-illuminated CCDs increased from pre-flight values near 10^{-6} to around 10^{-4}, while that of the 2 back-illuminated CCDs remained at about 10^{-5}. Several lines of evidence strongly support the conclusion that weakly penetrating radiation — relatively low-energy (0.1–0.5-MeV) protons — caused the CTI degradation of the front-illuminated CCDs:

1. The back-illuminated CCDs (charge-transfer channel behind 45-μm silicon) suffered little degradation.[8]
2. Detectible damage occurred only during radiation-belt passages when ACIS was in the focal position; none occurred when ACIS was in the next-in-line (NIL) position.
3. With the polyimide-backed High-Energy Transmission Gratings (HETG) inserted, the CCDs experienced no detectible degradation,[9] even when in the focal position during radiation-belt passages.
4. Serial-read-out (from the frame-store area) CTI is much less than parallel-read-out (into the frame-store area) CTI of the front-illuminated devices, demonstrating no damage to the shielded frame-store area.[8,10]
5. Despite the dramatic increase in the front-illuminated CCDs' CTI, dark current remained low, showing that damage does not extend significantly beyond the charge-transfer channel.[8,10]
6. Analysis[11,12] of ACIS spectra of Flight Contamination Monitor (FCM) sources[13,14] mounted in the telescope's forward contamination cover, show no degradation of energy resolution prior to door opening.
7. Irradiation (at NASA's Goddard Space Flight Center) of flight-like ACIS front-illuminated CCDs with 0.1–0.5-MeV protons, reproduces the behavior of the ACIS flight devices.[8,10]
8. Estimates of the radiation-belt proton fluence[15] combined with simulations of proton transport through the *Chandra* optical system[9] are consistent with the observed damage.

Pre-flight shielding analysis had shown that the focal-plane instruments are well-shielded against penetrating radiation. Unfortunately, this line-of-sight analysis did not treat scattering of weakly penetrating ions. The anomaly investigation concluded that, during radiation-belt transits, relatively low-energy ions Rutherford scatter off the mirrors onto the focal plane. The minimum proton energy to reach the charge-transfer channel, after penetrating ACIS's optical blocking filter (OBF) is about 0.1 MeV for an ACIS front-illuminated CCD and about 2 MeV for a back-illuminated one. Because the time-averaged proton spectrum is rather soft, it is the 0.1–0.5-MeV protons that effect the most displacement damage and degrade the CTI of the front-illuminated CCDs.

Protecting the *Chandra* science instruments against weakly penetrating radiation entering the telescope's aperture is straightforward: Move ACIS into next-in-line (NIL) position and power down video boards; with HRC now in the focus position, close the HRC door and ramp down or switch off all high voltage; and (optionally) retract the Objective Transmission Gratings (OTGs). Obviously, activating these radiation-protection procedures necessarily stops all science observations. Thus, we developed a radiation-management strategy (§3) to budget the residual CTI degradation over the mission lifetime.

3. RADIATION-MANAGEMENT STRATEGY

To preserve the scientific utility of ACIS's front-illuminated CCDs throughout the (> 10-y) mission, while minimizing lost observing time, we budgeted a 5%/y CTI increase for the front-illuminated CCDs. As reported previously,[7] the strategy for managing this radiation damage is three-tiered.

Scheduled protection. *Chandra* observations are scheduled weeks in advance, thus scheduled protection employs probabilistic models for the radiation environment to determine when to activate radiation protection. Currently, the planning system employs the standard AP8 model for flux thresholds and the *Chandra* Radiation Model (CRM, §4) for fluence thresholds. Because the fidelity of the AP8 model declines rapidly outside 6.6 $R_\oplus$ geocentric (36-Mm altitude), the scheduling pads the AP8-predicted radiation-protection radii, such that they are typically about 12–13 $R_\oplus$. Eventually, we hope to replace flux predictions from AP8 with those from an enhanced *Chandra* Radiation Model (CRM, §4).

Intervention. The intervention strategy employs real-time estimates of proton flux and fluence to decide whether to stop science at the next ground contact or earlier if needed. The *Chandra* operations team automatically monitors real-time data from the National Oceanographic and Atmospheric Administration (NOAA) Space Environment Center (SEC). Based upon these data combined with the CRM (§4) and the current science-instrument configuration, the *Chandra* X-ray Center (CXC) generates a real-time estimate of the proton flux and accrued and projected proton fluence. When these levels exceed pre-set thresholds, a computer-issued alert pages designated personnel to evaluate risk and determine a course of action.

Autonomous protection. Because communication with *Chandra* nominally occurs for only an hour every 8 hours, the *Chandra* flight computer watches radiation levels reported by the on-board radiation monitor — Electron, Proton, Helium Instrument[16] (EPHIN). If the reported radiation exceeds pre-set thresholds, the flight computer autonomously stops science and initiates radiation protection of the science instruments (see §2). Autonomous protection defends against rapid damage resulting from inadvertently transiting the radiation belt or enduring a severe solar-energetic-particle (SEP) event with ACIS unprotected. However, the EPHIN is not sensitive to the weakly penetrating protons causing most of the radiation damage to the front-illuminated CCDs.

4. CHANDRA RADIATION MODEL (CRM)

The strategy for managing radiation degradation relies upon real-time space-weather data (primarily from the NOAA/SEC) and upon a reasonably accurate model for the radiation environment in *Chandra*'s high elliptical orbit. To estimate proton fluence accumulated during radiation-belt transits, pre-existing radiation-environment tools and models — the European Space Agency (ESA) SPENVIS[17] (SPace ENVironment Information System) tool with the AP8 model, and the U.S. Air Force Research Laboratory (AFRL) CRRESPRO tool[18] with CRRES-EPAS (Combined Radiation and Release Effects Satellite - Electron and Proton Angle Spectrometer) data sets — yield mutually consistent, reliable results.[7] However, the *Chandra* X-ray Observatory spends about 85%–80% of its time outside the inner magnetosphere — i.e., in the outer magnetosphere (including the magnetotail), the magnetosheath, and the solar wind. To deal with this more-distant and complicated environment, we developed the *Chandra* Radiation Model[15] (CRM).

The CRM is a data-driven model, describing the global radiation environment — magnetosphere, magnetosheath, and solar wind. CRM1[15] utilized data from the Energetic Particles and Ion Composition[19] (EPIC) instrument on the *Geotail* satellite,[20, 21] operating (since 1995) in a low-inclination elliptical orbit with 8-$R_\oplus$ perigee and 30-$R_\oplus$ apogee. The more recent CRM2 adds data from the Comprehensive Energetic-Particle Pitch Angle Distribution[22] (CEPPAD) instrument on the *Polar* satellite,[23] operating in a high-inclination elliptical orbit with 2-$R_\oplus$ perigee and 9-$R_\oplus$ apogee. The CRM provides a probabilistic low-energy-proton environment for use in mission planning. In addition, the CRM also correlates the low-energy-proton environment to the planetary K index, K_p (a measure of geomagnetic activity). Figure 2 maps the low-energy-proton flux, for various levels of geomagnetic activity. Typically, $1 \leq K_p \leq 3$; $K_p \geq 5$ indicates a geomagnetic storm.

By propagating the *Chandra* orbit through the CRM environment, we estimate the external flux and fluence of 0.14-MeV protons — i.e., of those protons most damaging to ACIS front-illuminated CCDs. For planning purposes, we necessarily use the probabilistic CRM. However, for real-time estimation, we employ the K_p-correlated CRM, driven by NOAA/SEC-provided real-time data[24] from NASA's Advanced Composition Explorer[25] (*ACE*), in L1 orbit (0.01 Astronomical Units, or 235 $R_\oplus$, sunward of the earth).

The *ACE* Electron, Proton, and Alpha Monitor[26] (EPAM) P3 channel measures the intensity of 0.14-MeV protons. Thus, when *Chandra* is in the solar wind, we directly determine the flux (external to *Chandra*) of those protons most damaging to ACIS front-illuminated CCDs. As currently implemented, real-time estimation of the *Chandra* environment assumes that the 0.14-MeV-proton flux in the magnetosheath (between the bow shock and the magnetosphere) is twice the solar-wind value (to account for acceleration through the bow shock) plus the K_p-correlated CRM estimate for this region. Within the outer magnetosphere (inside the magnetopause), real-time estimation takes the K_p-correlated CRM estimate plus half the solar-wind value (to hedge against penetration of solar-wind protons into regions of the outer magnetosphere). We plan to improve the CRM by more accurately treating geomagnetic screening of the 0.14-MeV protons.

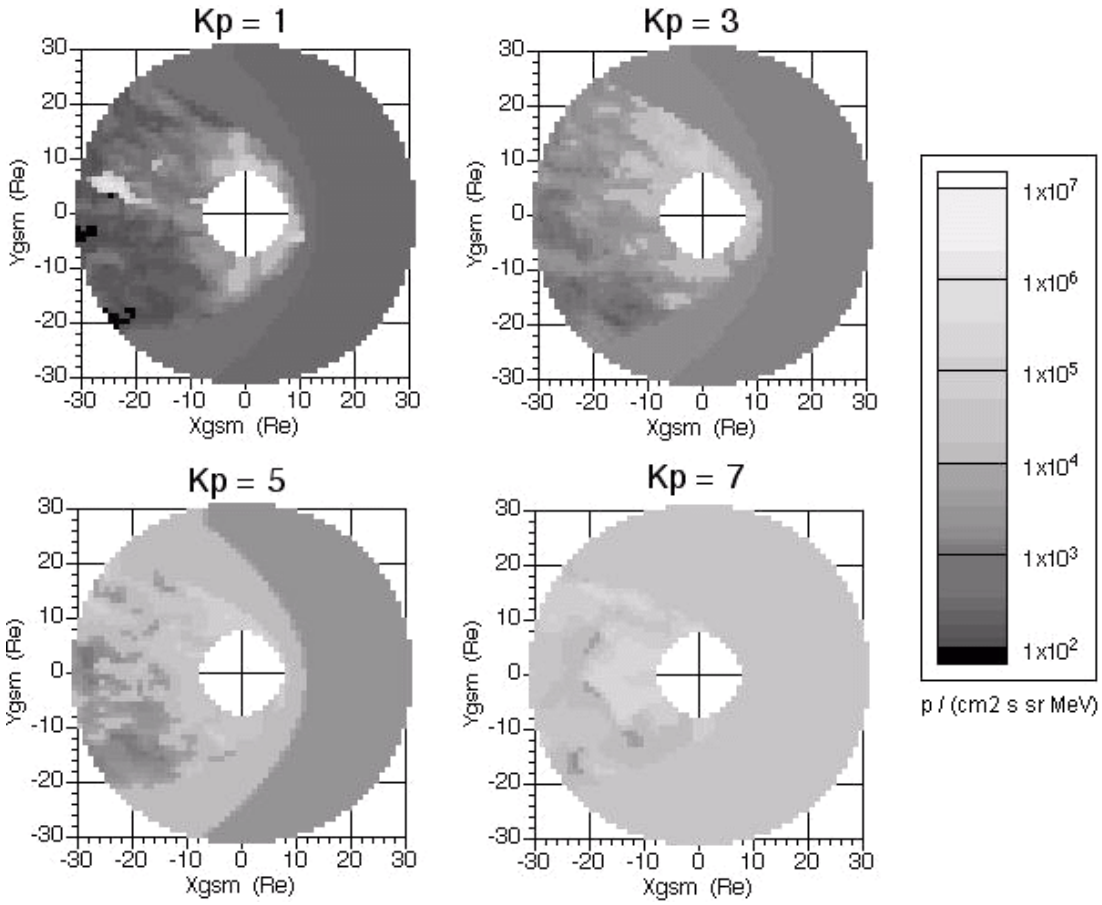

Figure 2. Chandra Radiation Model (CRM) map of 0.14-MeV-proton flux for various levels of geomagnetic activity. The natural coordinate system for the CRM is the Geocentric Solar Magnetospheric (GSM), specified by the earth–sun line and the transverse-projected earth magnetic-field axis. Note that the magnetospheric proton flux approximately doubles per unit increment of K_p. [Jacobs-Sverdrup/MSFC]

To drive the K_p-correlated CRM, we use the NOAA/SEC-provided Costello (neural-network) predictive K_p index.[27] The Costello neural net is trained to predict a value for K_p based upon solar-wind-plasma parameters. Accordingly, the NOAA/SEC uses real-time data from the *ACE* Solar-Wind Electron Proton Alpha Monitor[28] (SWEPAM) and the *ACE* Magnetic Fields Experiment[29] (MAG) to drive the K_p estimator.

5. CASE STUDY

To demonstrate the use of real-time data and tools in *Chandra* operations, we present a case study of a recent radiation event. In addition to the *ACE* EPAM, SWEPAM, and MAG real-time data discussed above (§4), the NOAA/SEC provides real-time data from the *ACE* Solar Isotope Spectrometer[30] (SIS), which measures the flux of high-energy (> 10 MeV) protons. The NOAA Geostationary Operational Environmental Satellite (GOES) system, in geosynchronous orbit (6.6 $R_\oplus$), also monitors these high-energy protons for solar-energetic-particle (SEP) events and solar-radiation storms. Other relevant GOES real-time data give the x-ray flux (monitoring solar x-ray flares) and the medium-energy-proton flux, which we have shown to correlate closely with the *Chandra* EPHIN proton flux in similar energy channels.[31]

The GOES x-ray monitor detected a large, moderate-duration x-ray flare (Figure 3, left) early on 2002:236 (August 24). Soon thereafter, the *ACE* SIS (Figure 4) and GOES high-energy particle monitor (Figure 3, right) detected a solar-energetic-particle (SEP) event associated with the x-ray flare. The NOAA/SEC issued automated alerts for the x-ray flare and for the solar-proton storm.

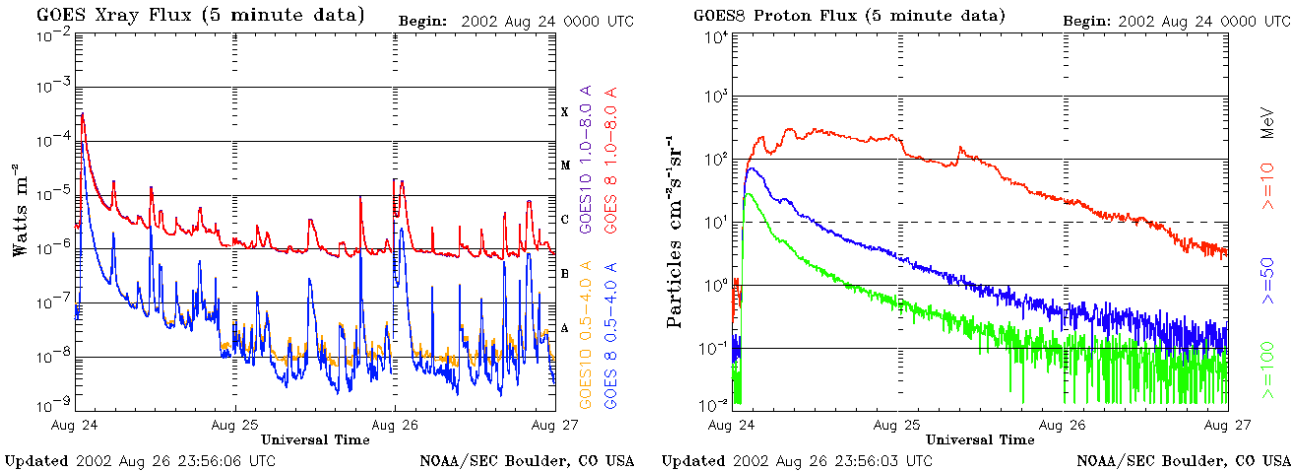

Figure 3. GOES x-ray (left panel) and high-energy-proton (right panel) data. Note the large (X3-class), moderate-duration x-ray flare at Aug-24 01 UT, followed by a moderate (S2) solar proton storm. [NOAA/SEC]

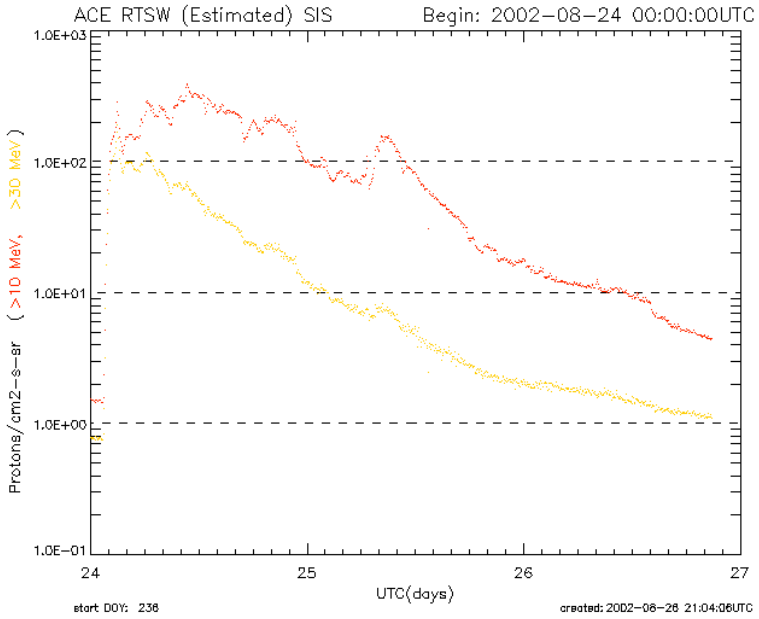

Figure 4. ACE SIS data. The ACE Solar Isotope Spectrometer measures high-energy nonthermal protons. Note the similarity of these data to the corresponding GOES proton data (Fig. 3, right). [NOAA/SEC]

Alerted to the onset of the solar radiation storm, we sought to determine whether it had triggered autonomous radiation protection of the *Chandra* science instruments. Of EPHIN's 4 electron, 4 proton, and 4 alpha channels, the flight computer currently monitors the (4.3–7.8-MeV) P4GM, (41–53-MeV) P41GM, and (2.6–6.2-MeV) E1300 for triggering radiation protection. Lacking continuous contact with the *Chandra* spacecraft, we estimated the *Chandra* EPHIN proton fluxes based upon NOAA/SEC-provided data from the GOES-8 moderate-energy proton channels. Figure 5 indicated and subsequent telemetry confirmed that radiation protection had been activated, so the *Chandra* operations team began re-planning.

Two basic considerations govern the decision as to when to re-start science operations. First, the moderate- and high-energy proton flux must be sufficiently low to avoid autonomous triggering of radiation protection. Second, the projected low-energy proton fluence should not exceed that budgeted for such events. By Aug-25 mid-day UT, the GOES-estimated EPHIN flux (Figure 5), as well as EPHIN data telemetered during ground

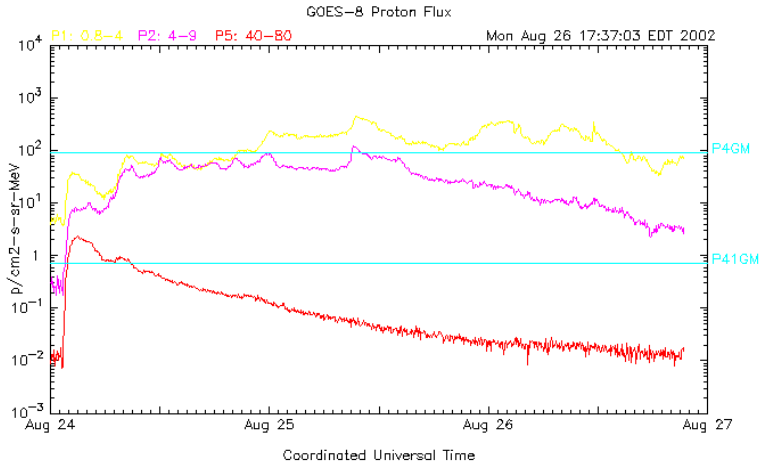

Figure 5. GOES-8 proton channels corresponding to *Chandra*-EPHIN proton channels used to autonomously trigger radiation protection. Typically, protons more energetic than 5 MeV have sufficient rigidity to reach geosynchronous orbit, thus GOES-8 predicts EPHIN rates. Note that the GOES-P5 flux crosses the EPHIN-P41GM threshold shortly after on-set of the solar-energetic-particle (SEP) event, suggesting activation of autonomous radiation protection. [CXC/SOT]

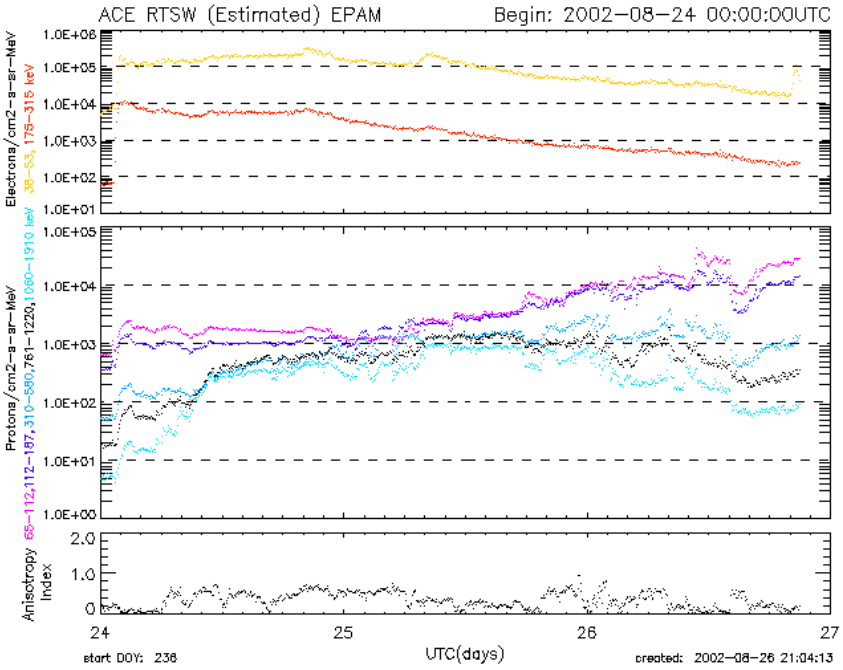

Figure 6. ACE EPAM data. The ACE Electron, Proton, Alpha Monitor measures low-energy suprathermal protons and electrons. Note particularly the gradual increase in soft-proton flux following the solar-energetic-particle (SEP) event of Aug-24 02 UT (Fig. 4 and Fig. 3, right). [NOAA/SEC]

contacts, showed that autonomous triggering of radiation protection would not occur. Projecting the low-energy-proton fluence is typically much less certain. This is because these protons are quasi-trapped in the coronal mass ejection (CME) and, thus, typically increase in intensity over the 2–3 days required for the thermal-plasma ejecta to reach the earth and for its shock front to pass. Furthermore, geomagnetic activity (effected by the solar-wind thermal plasma) enhances the proton flux in the magnetosphere, and the geomagnetic field screens solar-wind low-energy protons from parts of the magnetosphere.

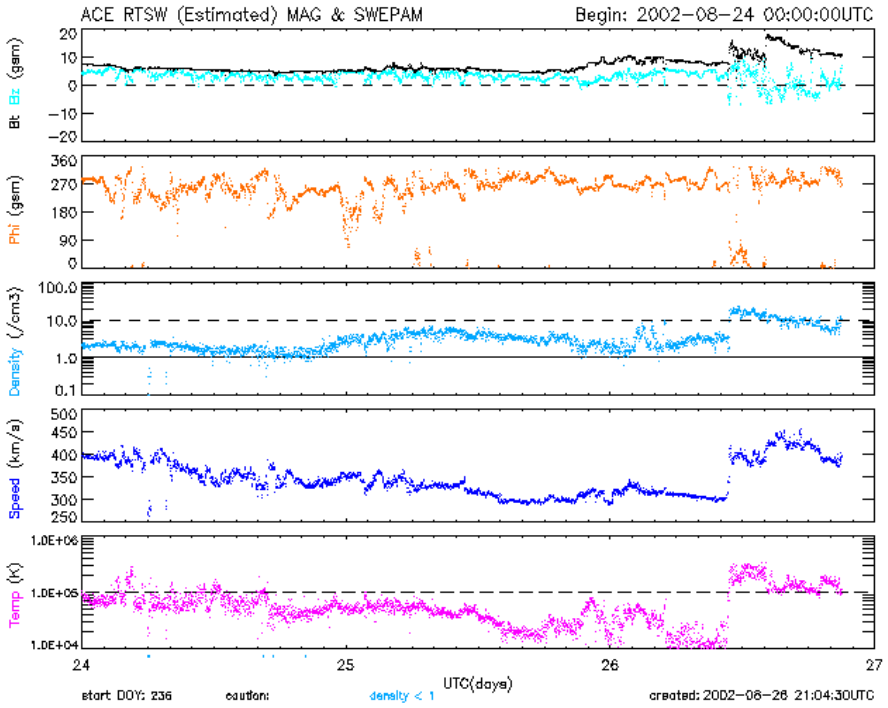

Figure 7. ACE MAG-SWEPAM data. The ACE Magnetometer and Solar-Wind Electron, Proton, Alpha Monitor measure the magnetic field and properties of the solar-wind thermal plasma. Note the weak shock passing ACE at Aug-26 10:40 UT, associated with the Aug-24 coronal mass ejection (CME). [NOAA/SEC]

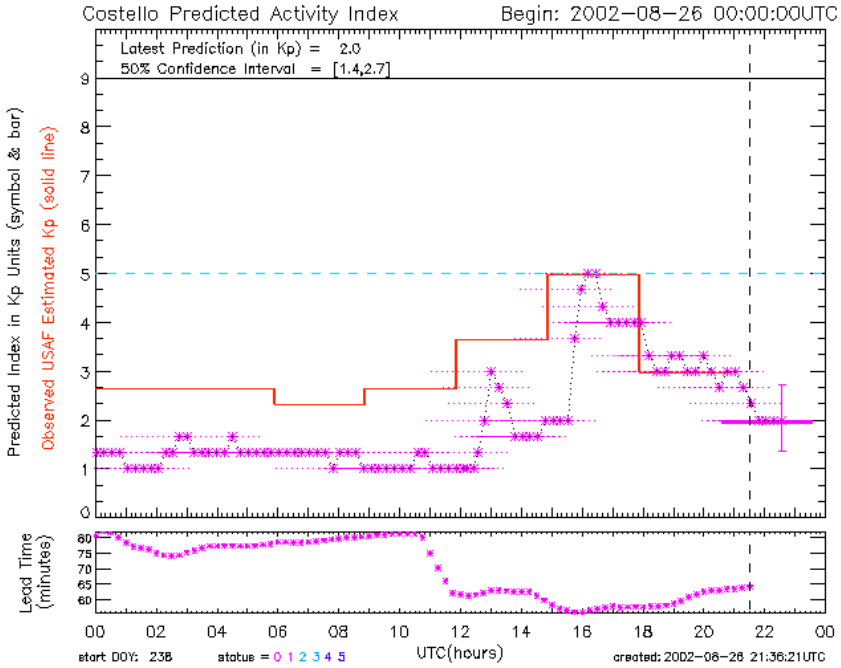

Figure 8. Costello K_p predictor of geomagnetic activity. ACE MAG-SWEPAM data (Fig. 7) drive a neural-net estimator of geomagnetic activity (*). The solid line compares the USAF quick-look K_p, based upon 3-hour ground-station magnetometer variations. Note the minor (G1) geomagnetic storm triggered by the shock (Fig. 7). [NOAA/SEC]

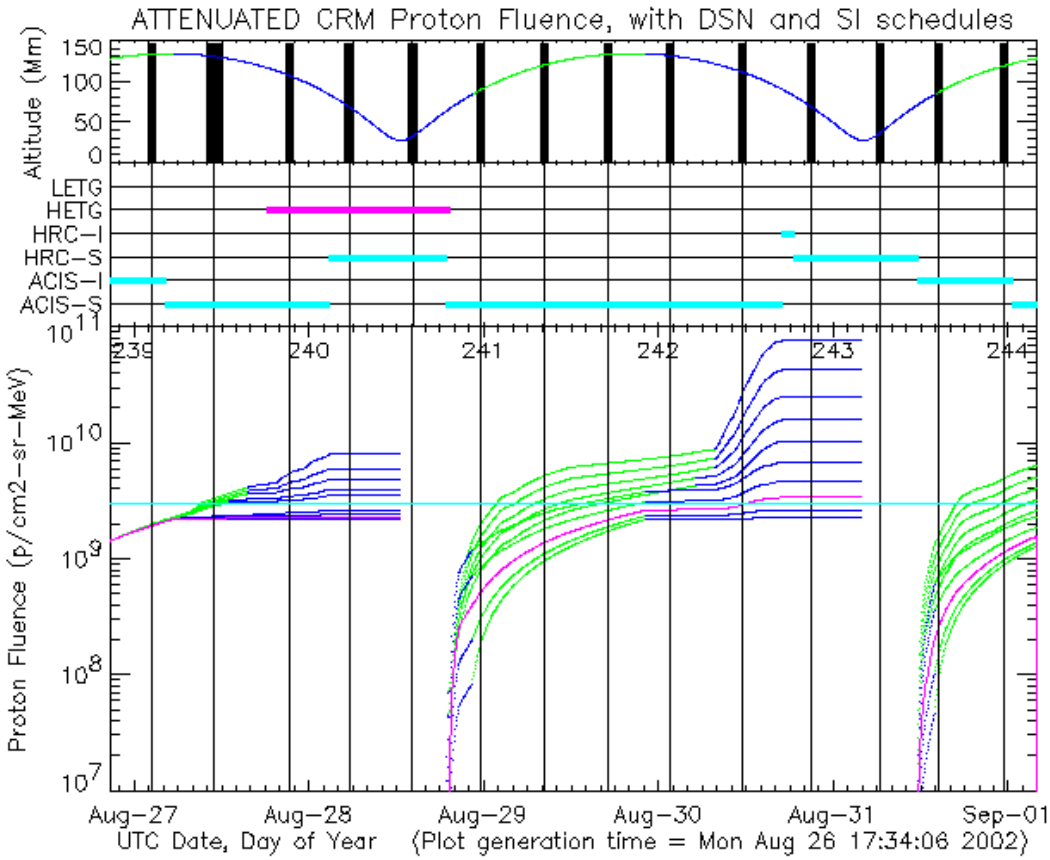

Figure 9. Chandra Radiation Model estimate of external fluence of 0.14-MeV protons, appropriately attenuated based upon instrument configuration. Note that the projected orbital fluence until the Aug-28 perigee is close to the budgeted allocation of 3×10^9 p/(cm^2 sr MeV). [CXC/SOT]

The real-time *Chandra* Radiation Model (CRM, §4)) uses as input the solar-wind 0.14-MeV-proton flux from the *ACE* EPAM P3 channel (Figure 6) and, driven by the *ACE* SWEPAM and MAG data (Figure 7), the Costello K_p predictor (Figure 8). Given the solar-wind proton flux and the geomagnetic index K_p, the CRM estimates the 0.14-MeV-proton environment globally — in the solar wind, in the magnetosheath, and in the outer magnetosphere.

Finally, the *Chandra* operations team automatically propagates the *Chandra* orbit through the real-time CRM environment, to estimate the projected accumulated 0.14-MeV-proton (external) fluence for the orbit. The "attenuated" external fluence (Figure 9) includes a relative transmission factor dependent upon the science-instrument configuration. Based in part upon numerical simulations,[9] the relative transmission to ACIS is 1 for the bare ACIS, 0.5 for LETG–ACIS, 0.2 for HETG–ACIS, and 0 for ACIS in the next-in-line (NIL) position — i.e., HRC in the focal position. Figure 9 shows that the CRM-projected orbital fluence was below the budgeted allocation of 3.0×10^9 0.14-MeV-p/(cm^2 sr MeV) — about 0.1% of the (attenuated) external fluence accumulated during the 8 unprotected radiation-belt passes.

6. CTI STATUS AND MODEL COMPARISON

Since implementing radiation-damage management, the mean CTI (measured with focal plane at −120°C, in Mn-Kα) of the I-array (front-illuminated) CCDs increased from 125×10^{-6} to 134×10^{-6} at an average rate of 3.4×10^{-6} (2.7%) per year (Figure 10, left). That of the S3 (back-illuminated) CCD increased from 14×10^{-6} to 18×10^{-6} at an average rate of 1.3×10^{-6} (9.2%) per year (Figure 10, right). Thus, both the front-illuminated and the back-illuminated CCDs will remain scientifically useful throughout the *Chandra* mission.

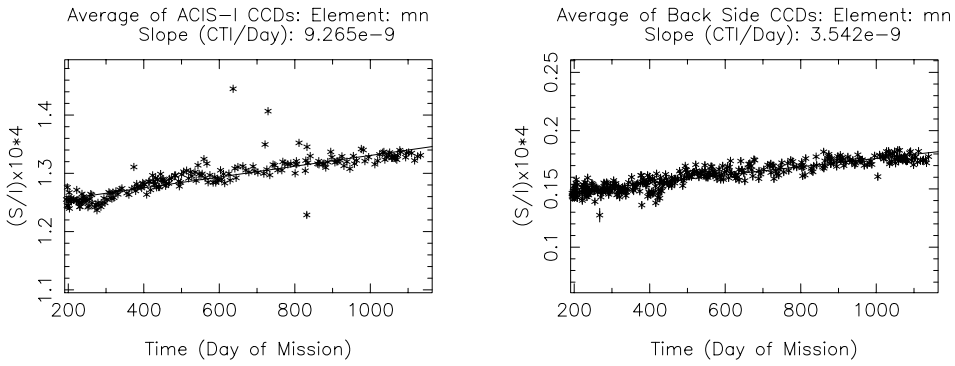

Figure 10. CTI of ACIS's 4 I-array front-illuminated CCDs (left panel) and of the central S-array back-illuminated CCD (right panel). Displayed CTIs are measured in Mn-Kα at a -120°C focal-plane temperature. [CXC/SOT]

Using the AP8 model, we determined that the external proton fluence accumulated during the 8 unprotected radiation-belt passages was 3.0×10^{12} p/(cm^2 sr MeV) at 0.14 MeV. This provides a normalization of the front-illuminated CTI increase to the AP8-derived external proton fluence — 4.2×10^{-17} per (AP8) 0.14-MeV-p/(cm^2 sr MeV). Since implementing radiation-damage management, the CRM-estimated (attenuated) external proton fluence has increased at 0.09×10^{12} per year. Thus, we obtain a normalization of the subsequent front-illuminated CTI increase to the CRM-derived (attenuated) external proton fluence — 4.0×10^{-17} per (CRM) 0.14-MeV-p/(cm^2 sr MeV). Although the exceptionally close agreement of these normalizations is clearly fortuitous, it does indicate that the CRM is adequately estimating the *Chandra* low-energy-proton environment.

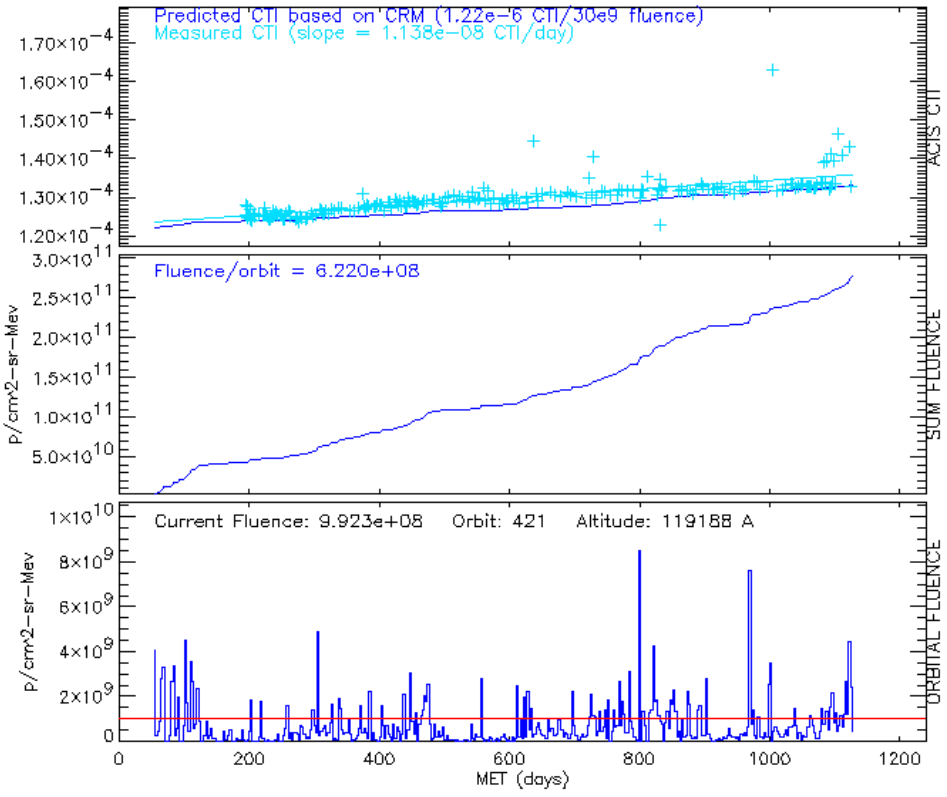

Figure 11. Comparison of CTI increase versus CRM estimates of 0.14-MeV-proton fluence. Note (top panel) the agreement between the CTI slope measured (+) and that predicted by scaling the radiation models. [CXC/SOT]

Acknowledgements

For their contributions to resolving the ACIS CTI anomaly, we thank colleagues at AFRL, MIT, and University Kiel (Germany), as well as in our respective organizations. We also appreciate the generous help of personnel at the NOAA Space Environment Center, *ACE* Science Center (Cal Tech), *ACE* Operations Center (GSFC), Johns Hopkins University Applied Physics Laboratory (JHU/APL), Boston University (BU), University of Iowa, and Rice University. In particular, we thank the *Geotail* EPIC team (JHU/APL) and the *Polar* CEPPAD team (BU) for providing access to their data sets.

REFERENCES

1. M. C. Weisskopf, H. D. Tananbaum, L. P. Van Speybroeck, and S. L. O'Dell, "Chandra X-ray Observatory: Overview," in *X-Ray Optics, Instruments, and Missions*, J. Trümper and B. Aschenbach, eds., *Proc. SPIE* **4012**, pp. 2–16, 2000.
2. M. C. Weisskopf, B. Brinkman, C. Canizares, G. Garmire, S. Murray, and L. P. Van Speybroeck, "An Overview of the Performance and Scientific Results from the Chandra X-Ray Observatory (CXO)," *PASP* **114**, pp. 1–24, 2002.
3. S. S. Murray, J. H. Chappell, A. T. Kenter, K. Kobayashi, R. P. Kraft, G. R. Meehan, M. V. Zombeck, G. W. Fraser, J. F. Pearson, J. E. Lees, A. N. Brunton, S. E. Pearce, M. Barbera, A. Collura, and S. Serio, "AXAF High-Resolution Camera (HRC)," in *EUV, X-Ray, and Gamma-Ray Instrumentation for Astronomy VIII*, O. H. Siegmund and M. A. Gummin, eds., *Proc. SPIE* **3114**, pp. 11–25, 1997.
4. S. S. Murray, G. K. Austin, J. H. Chappell, J. J. Gomes, A. T. Kenter, R. P. Kraft, G. R. Meehan, M. V. Zombeck, G. W. Fraser, and S. Serio, "In-flight performance of the Chandra High-Resolution Camera," in *X-Ray Optics, Instruments, and Missions*, J. Trümper and B. Aschenbach, eds., *Proc. SPIE* **4012**, pp. 68–80, 2000.
5. B. E. Burke, J. Gregory, M. W. Bautz, G. Y. Prigozhin, S. E. Kissel, B. B. Kosicki, A. H. Loomis, and D. J. Young, "Soft x-ray CCD imagers for AXAF," *I.E.E.E. Trans. Elec. Devices* **44**, pp. 1633–1642, 1997.
6. M. W. Bautz, M. Pivovaroff, F. Baganoff, T. Isobe, S. E. Jones, S. E. Kissel, B. Lamarr, H. L. M. G. Y., P. G. R., Ricker, J. A. Nousek, C. E. Grant, K. Nishikida, F. Scholze, R. Thornagel, and G. Ulm, "X-ray CCD calibration for the AXAF CCD Imaging Spectrometer," in *X-Ray Optics, Instruments, and Missions*, R. B. Hoover and A. B. Walker, eds., *Proc. SPIE* **3444**, pp. 210–224, 1998.
7. S. L. O'Dell, , M. W. Bautz, W. C. Blackwell, Y. M. Butt, R. A. Cameron, R. F. Elsner, M. S. Gussenhoven, J. J. Kolodziejczak, J. I. Minow, R. M. Suggs, D. A. Swartz, A. F. Tennant, S. N. Virani, and K. M. Warren, "Radiation environment of the Chandra X-ray Observatory," in *X-Ray and Gamma-Ray Instrumentation for Astronomy XI*, K. A. Flanagan and O. H. W. Siegmund, eds., *Proc. SPIE* **4140**, pp. 99–110, 2000.
8. G. Y. Prigozhin, S. E. Kissel, M. W. Bautz, C. Grant, B. LaMarr, R. F. Foster, G. R. Ricker, and G. P. Garmire, "Radiation damage in the Chandra x-ray CCDs," in *X-Ray Optics, Instruments, and Missions*, J. Trümper and B. Aschenbach, eds., *Proc. SPIE* **4012**, pp. 720–730, 2000.
9. J. J. Kolodziejczak, R. F. Elsner, R. A. Austin, and S. L. O'Dell, "Ion transmission to the focal plane of the Chandra X-ray Observatory," in *X-Ray and Gamma-Ray Instrumentation for Astronomy XI*, K. A. Flanagan and O. H. W. Siegmund, eds., *Proc. SPIE* **4140**, pp. 135–143, 2000.
10. G. Y. Prigozhin, M. W. Bautz, C. Grant, S. E. Kissel, B. LaMarr, and G. R. Ricker, "Characterization of the radiation damage in the Chandra x-ray CCDs," in *X-Ray and Gamma-Ray Instrumentation for Astronomy XI*, K. A. Flanagan and O. H. W. Siegmund, eds., *Proc. SPIE* **4140**, pp. 123–134, 2000.
11. R. F. Elsner, J. J. Kolodziejczak, S. L. O'Dell, D. A. Swartz, A. F. Tennant, and M. C. Weisskopf, "Measurements with the Chandra X-ray Observatory's flight contamination monitor," in *X-Ray Optics, Instruments, and Missions*, J. Trümper and B. Aschenbach, eds., *Proc. SPIE* **4012**, pp. 612–618, 2000.
12. R. F. Elsner, J. J. Kolodziejczak, S. L. O'Dell, D. A. Swartz, A. F. Tennant, and M. C. Weisskopf, "Measurements with the Chandra X-ray Observatory's flight contamination monitor," in *X-Ray Optics, Instruments, and Missions IV*, R. B. Hoover and A. B. Walker, eds., *Proc. SPIE* **4138**, pp. 1–9, 2000.

13. R. F. Elsner, M. K. Joy, S. L. O'Dell, B. D. Ramsey, and M. C. Weisskopf, "Ground-to-orbit transfer of the AXAF-I flux scale: In-situ contamination monitoring of x-ray telescopes," in *Multilayer and grazing incidence X-ray/EUV optics for astronomy and projection lithography*, R. B. Hoover and A. B. Walker, eds., *Proc. SPIE* **2279**, pp. 332–342, 1994.
14. R. F. Elsner, S. L. O'Dell, B. D. Ramsey, A. F. Tennant, M. C. Weisskopf, J. J. Kolodziejczak, D. A. Swartz, D. E. Engelhaupt, G. P. Garmire, J. A. Nousek, M. W. Bautz, T. J. Gaetz, and P. Zhao, "Calibration results for the AXAF flight contamination monitor," in *X-Ray Optics, Instruments, and Missions*, R. B. Hoover and A. B. Walker, eds., *Proc. SPIE* **3444**, pp. 177–188, 1998.
15. W. C. Blackwell, J. I. Minow, K. Warren, R. M. Suggs, S. L. O'Dell, D. A. Swartz, A. F. Tennant, and S. N. Virani, "Modeling the Chandra space environment," in *X-Ray and Gamma-Ray Instrumentation for Astronomy XI*, K. A. Flanagan and O. H. W. Siegmund, eds., *Proc. SPIE* **4140**, pp. 111–122, 2000.
16. R. Müller-Mellin, H. Kunow, V. Fleissner, E. Pehlke, E. Rode, N. Roschmann, C. Scharmberg, H. Sierks, P. Rusznyak, I. E. S. McKenna-Lawlor, J. Sequeiros, D. Meziat, S. Sanchez, J. Medina, L. der Peral, M. Witte, R. Marsden, and J. Henrion, "COSTEP — comprehensive suprathermal and energetic particle analyzer," *Solar Physics* **162**, pp. 483–504, 1995.
17. D. Heynderickx, B. Quaghebeur, B. Fontaine, A. Glover, W. C. Carey, and E. J. Daly, "New features of ESA's Space Environment Information System (SPENVIS)." ESA Workshop on Space Weather, 1999.
18. M. S. Gussenhoven, E. G. Mullen, M. D. Violet, C. Hein, J. Bass, and D. Madden, "CRRES high-energy proton flux maps," *IEEE Trans. Nuclear Science* **40**, pp. 1450–1457, 1993.
19. D. J. Williams, R. W. McEntire, C. Schlemm II, A. T. Y. Lui, G. Gloeckler, S. P. Christon, and F. Gliem, "Geotail Energetic Particles and Ion Composition instrument," *J. Geomag. Geoelect.* **46**, pp. 39–57, 1994.
20. A. Nishida, K. Uesugi, I. Nakatani, T. Mukai, D. H. Fairfield, and M. H. Acuna, "Geotail mission to explore earth's magnetotail," *Eos* **73**, pp. 425–427, 1992.
21. A. Nishida, "The Geotail mission," *Geophysical Research Letters* **21**, pp. 2871–2873, 1994.
22. H. Spence and J. Blake, "First observations by the CEPPAD imaging proton spectrometer aboard Polar," *Advances in Space Research* **20**, pp. 933–936, 1998.
23. R. A. Hoffman, "Polar —from the top down," *Advances in Space Research* **20**, pp. 569–573, 1997.
24. R. D. Zwickl, K. A. Doggett, S. Sahm, W. P. Barrett, R. N. Grubb, T. R. Detman, V. J. Raben, C. W. Smith, P. Riley, R. E. Gold, R. A. Mewaldt, and S. Maruyama, "The NOAA Real-Time Solar-Wind (RTSW) system using ACE data," *Space Science Reviews* **86**, pp. 633–648, 1998.
25. E. C. Stone, A. M. Frandsen, R. A. Mewaldt, E. R. Christian, D. Margolies, J. F. Ormes, and F. Snow, "The Advanced Composition Explorer," *Space Science Reviews* **86**, pp. 1–22, 1998.
26. R. E. Gold, S. M. Krimigis, S. E. Hawkins III, D. K. Haggerty, D. A. Lohr, E. Fiore, T. P. Armstrong, G. Holland, and L. J. Lanzerotti, "Electron, Proton and Alpha Monitor on the Advanced Composition Explorer spacecraft," *Space Science Reviews* **86**, pp. 541–562, 1998.
27. K. A. Costello, "Moving the Rice MSFM into real-yime forecast mode using solar-wind driven forecast models." Ph. D. dissertation, Rice University, June 1997.
28. D. J. McComas, S. J. Bame, P. Barker, W. C. Feldman, J. L. Phillips, P. Riley, and J. W. Griffee, "Solar Wind Electron Proton Alpha Monitor (SWEPAM) for the Advanced Composition Explorer," *Space Science Reviews* **86**, pp. 563–612, 1998.
29. C. W. Smith, J. L. Heureux, N. F. Ness, M. H. Acuña, L. F. Burlaga, and J. Scheifele, "The ACE magnetic fields experiment," *Space Science Reviews* **86**, pp. 613–632, 1998.
30. E. C. Stone, C. M. S. Cohen, W. R. Cook, A. C. Cummings, B. Gauld, B. Kecman, R. A. Leske, R. A. Mewaldt, M. R. Thayer, B. L. Dougherty, R. I. Grumm, B. D. Milliken, R. G. Radocinski, M. E. Wiedenbeck, E. R. Christian, S. Shuman, and T. T. von Rosenvinge, "The Solar Isotope Spectrometer for the Advanced Composition Explorer," *Space Science Reviews* **86**, pp. 357–408, 1998.
31. S. N. Virani, R. A. Cameron, P. P. Plucinsky, R. Mueller-Mellin, and S. L. O'Dell, "Monitoring the Chandra X-ray Observatory radiation environment: Correlations between GOES-8 and Chandra/EPHIN during DOY 89-106, 2001," in *Multi-Wavelength Observations of Coronal Structure and Dynamics — Yohkoh 10th Anniversary Meeting*, P. C. H. Martens and D. Cauffman., eds., *COSPAR Colloquia Series* **to be published**, 2002.